THE JOURNAL OF PHYSICAL CHEMISTRY A

Article

pubs.acs.org/JPCA

Disputed Mechanism for NIR-to-Red Upconversion Luminescence in $NaYF_4:Yb^{3+},Er^{3+}$

Mary T. Berry* and P. Stanley May

Department of Chemistry, University of South Dakota Vermillion, South Dakota 57069, United States

Supporting Information

ABSTRACT: The most commonly proposed mechanisms for NIR-to-red upconversion in the well-studied material β-$NaYF_4:Er^{3+},Yb^{3+}$ are evaluated in order to resolve inconsistencies that persist in the literature. Each of four possible mechanisms is evaluated in terms of the direct analysis of spectroscopic data. It is shown that there are no important mechanisms that involve the first excited state of Er^{3+}, $^4I_{13/2}$, as an intermediate state. A large body of evidence overwhelmingly supports the proposed mechanism of Anderson et al., which suggests an intimate connection between NIR-to-red and NIR-to-blue upconversion. Namely, both red and blue upconversion are produced primarily by a three-photon excitation process that proceeds through the green emitting state to a dense manifold of states, $^4G/^2K$, above the blue emitting state, $^2H_{9/2}$. Competing relaxation mechanisms out of $^4G/^2K$ determine the relative amounts of blue and red upconversion produced. Multiphonon relaxation from $^4G/^2K$ results in blue upconversion, whereas back energy transfer from $Er^{3+}(^4G/^2K)$ to $Yb^{3+}(^2F_{7/2})$ results in red emission.

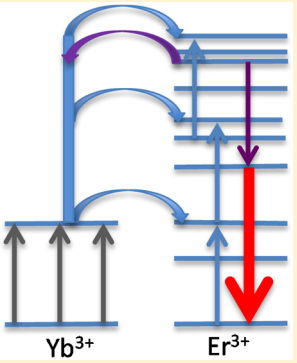

INTRODUCTION

NIR(λ_{ex} = 1 μm)-to-visible upconversion (UC) in Er^{3+}, Yb^{3+} codoped inorganic hosts has been the subject of very active research in recent years, particularly with the advent of methods for synthesizing highly dispersible upconverting nanomaterials.[1] The most active area is for the hexagonal-phase $NaYF_4$ host materials, often designated as β-$NaYF_4$. This host supports the most efficient documented upconversion efficiency, although, at low pump power densities, the La_2O_2S host is reported to be superior.[2] The mechanism for upconverting from NIR excitation to green emission was established by Auzel in 1966 as a two-step Yb → Er energy transfer upconversion (ETU) process, as illustrated in Figure 1.[3−5] For efficient upconversion, rapid energy migration among the Yb^{3+} ions is required. The two Yb^{3+} ground state absorption (GSA) events in Figure 1 do not generally occur at the same Yb^{3+} center, or even at Yb^{3+} ions that are nearest neighbors to Er^{3+}, but rather, the energy migrates from the absorption site to Yb^{3+} that are adjacent to the Er^{3+} upconversion centers. Thus, the Yb^{3+} energy-level diagram in Figure 1 represents the bath of Yb^{3+} in the lattice, whereas the Er^{3+} energy-level diagram represents a single Er^{3+} ion. For the remainder of this paper, Yb^{3+} participation will be assumed, but the Yb^{3+} energy levels will not be explicitly shown in the diagrams.

β-$NaYF_4$:Er,Yb upconverting materials also produce significant red emission with intensity comparable to that of the green emission when pump power densities (cw) exceed approximately 5 W/cm^2.[2,5−7] Unlike the mechanism for green emission, the mechanism for red upconversion is not universally agreed upon. The published data and accompanying arguments have not firmly established any particular mechanism as dominant, or confirmed whether multiple mechanisms are in play. As a result, inconsistencies in assigning the red upconversion mechanism persist in the literature, even for the well-studied host material, $NaYF_4$.[6−10] Part of the barrier to reaching agreement with regard to the mechanism is related to the complexity and abstract nature of the arguments, which are based on modeling excitation dynamics deduced from time-resolved luminescence measurements.

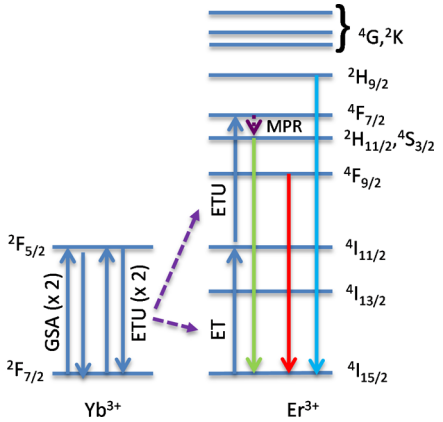

Figure 1. Well-established mechanism for production of green UC luminescence involves ground state absorption (GSA) by Yb^{3+} followed by two-step energy transfer upconversion (ETU) to Er^{3+}. This provides initial population of $Er(^4F_{7/2})$ which rapidly relaxes to populate $^2H_{11/2}$,$^4S_{3/2}$, the green emitting states. There are several proposed mechanisms for the origin of the observed red and blue UC luminescence.

In this paper, we evaluate the four most commonly cited mechanisms for red upconversion emission in terms of

Received: August 26, 2015
Published: September 1, 2015

DOI: 10.1021/acs.jpca.5b08324
J. Phys. Chem. A 2015, 119, 9805−9811

straightforward experiments, which can be interpreted without reliance on the indirect implications of complex mathematical models. These experiments strongly support one dominant three-photon mechanism for NIR-to-red upconversion emission in β-$NaYF_4$:Yb^{3+},Er^{3+}.

EXPERIMENTAL SECTION

Materials. Phase-pure, micrometer-scale powders of β-$NaYF_4$/18% Yb^{3+}, 2%Er^{3+} were obtained from Lorad Chemical Corporation. The material consisted of rod-shaped crystallites, as determined by SEM. Phase purity was assessed with powder XRD. SEM and XRD results for this sample are published in ref 6. Spectroscopic measurements were performed on packed, optically dense powders.

Nanocrystals of β-$NaYF_4$:17%Yb,x%Er (x = 0.03, 1, 3) were synthesized as described previously.[11] Briefly, a total of 0.50 mmol of lanthanide acetates was dissolved in 6 mL of oleic acid. The mixture was dried under vacuum at 100 °C for 1 h. The fluoride-containing solution was prepared by dissolving 1 mmol of sodium acetate and 2 mmol of sodium fluoride in 2 mL of oleic acid and 10 mL of 1-octadecene. This mixture was also dried under vacuum (100 °C; 30 min). The fluoride solution was then heated to 320 °C under Ar flow, at which point the lanthanide solution was injected within a span of 1 min. The reaction temperature was maintained for 30 min under Ar, and then allowed to cool to room temperature. Nanocrystals were precipitated with acetone and collected by centrifugation at 5000 rpm. Samples were then dispersed in toluene and reprecipitated twice more. For spectroscopic measurements, the nanoparticles were dispersed in toluene. The phase purity of the particles was confirmed by XRD and the particle size, as determined by TEM, was approximately 90 nm.

Spectroscopic Measurements. Pulsed excitation at 442 and 378 nm was provided by a dye laser (Laser Photonics DL-14) pumped by a nitrogen-gas laser (Laser Photonics UV-14). Pulsed excitation at 520 nm was provided by a type-II optical parametric oscillator system (Opolette 355, OPOTEK, Inc.). Pulsed excitation at 943 nm was provided by a dye laser (ND6000, Continuum) pumped by the second harmonic of a Nd:YAG laser (Surelite I, Continuum). Excitation at 943 nm was chosen because it lies on the high-energy side of the 976 nm absorbance maximum, which allowed collection of the majority of the Yb^{3+}: $^2F_{5/2} \rightarrow {}^2F_{7/2}$ emission spectrum without interference from laser scatter.

Except for the spectra shown in Figures 1 and 10, emission spectra were acquired with a 1/3m monochromator (Jobin-Yvon, Triax 320) equipped with a UV−vis-NIR photomultiplier tube (Hamamatsu, R2658P) in a cooled housing (Products for Research) on the axial exit port and a cooled NIR photomultiplier module (Hamamatsu H10330A-75) on the lateral exit port. Luminescence signal was detected using time-resolved photon counting by feeding the preamplified (SR 445A, SRS) detector output into a multichannel scalar (SR 430, SRS). The emission spectra in Figures 2 and 10 were collected using a miniature spectrometer (BLUE-Wave, StellarNet).

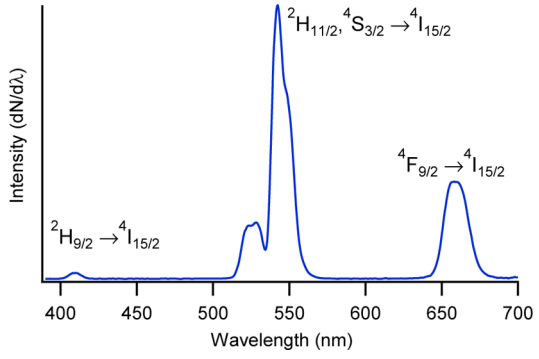

Figure 2. Visible upconversion emission spectrum of β-$NaYF_4$:18%Yb, 2%Er powders. Excitation was provided by a pulsed source at 943 nm.

Excitation spectra were acquired using a commercial fluorometer (Fluoromax 4, Horiba).

Diffuse reflectance spectra were acquired using a UV−vis-NIR dual beam absorbance spectrophotometer (Cary 5000, Agilent) equipped with a diffuse reflectance accessory (Praying Mantis, Harrick).

RESULTS AND DISCUSSION

Before evaluating the specific mechanisms for red upconversion, it is useful to present data which illustrate some of the well-accepted properties of this system which will then be used in our subsequent analysis. Figure 2 shows the visible upconversion emission spectrum from β-$NaYF_4$:18%Yb,2%Er powders. Red upconversion corresponds to the Er^{3+}: $^4F_{9/2} \rightarrow {}^4I_{15/2}$ transition, green upconversion to $^2H_{11/2}$, $^4S_{3/2} \rightarrow {}^4I_{15/2}$, and blue upconversion to $^2H_{9/2} \rightarrow {}^4I_{15/2}$, as illustrated in the energy-level diagrams of Figure 1.

The dependence of upconversion intensity, I, on excitation power density, P_{exc}, can be expressed as

$$I \propto P_{exc}^{n} \tag{1}$$

The value of the exponent, n, is generally power dependent and tends to decrease as P_{exc} increases.[12] At low values of P_{exc}, n approaches the true value of the number of photons involved in the excitation process. Eq 1 is often expressed in logarithmic form, as follows.

$$\log(I) = n\cdot\log(P_{exc}) + \text{const} \tag{2}$$

The value of n, therefore, is equal to the slope of a plot of $\log(I)$ vs $\log(P_{exc})$. Over relatively narrow ranges of P_{exc}, n is approximately constant, and the plot is a straight line. Over larger ranges of P_{exc}, however, a plot of $\log(I)$ vs $\log(P_{exc})$ exhibits significant curvature.[12]

Figure 3 (left panel) shows a plot of $\log(I)$ vs $\log(P_{exc})$ for upconversion emission in β-$NaYF_4$:18%Yb^{3+}, 2%Er^{3+} using NIR excitation at 943 nm. The slopes of the plots of $\log(I)$ vs $\log(P_{exc})$ are used to determine the exponent, n, for the dependence of the visible upconversion intensity on $\log(P_{exc})$ (See right panel, Figure 3). As expected, the value of n decreases with increasing power. Over the range of P_{exc} studied here, $n_{blue} > n_{red} > n_{green}$. Both red and blue upconversion are more sensitive to excitation power than green, and blue is more sensitive than red, especially at higher values of P_{exc}. Referring again to the right panel of Figure 3, extrapolation to low values of P_{exc} implies that green upconversion is produced via a two-photon process, and red and blue upconversion via three-photon processes.

The dependence of the red-to-green upconversion ratio, R/G, on P_{exc} is well documented in the literature, as is the fact that $n_{red} > n_{green}$.[7] As a result, it is widely accepted that a three-photon mechanism is active in red upconversion. What is not firmly established is the nature of the three-photon mechanism, and whether a two-photon mechanism also makes a significant contribution to red upconversion.

The first proposed mechanism to be evaluated here is the two-photon mechanism illustrated in the first panel of Figure 4. In this mechanism, the green emitting states, $^2H_{11/2}$ and $^4S_{3/2}$, are populated via the accepted ETU mechanism for green upconversion (see Figure 1), and the red emitting state, $^4F_{9/2}$, is subsequently populated via $^2H_{11/2}$, $^4S_{3/2} \rightarrow {}^4F_{9/2}$ multiphonon relaxation, MPR. The contribution from this mechanism can be evaluated with a down conversion experiment. Excitation directly above the green emitting state, $^4S_{3/2}$, $^2H_{11/2}$, into the $^4F_{7/2}$ level at 442 nm results in very weak red emission, relative

DOI: 10.1021/acs.jpca.5b08324
J. Phys. Chem. A 2015, 119, 9805−9811

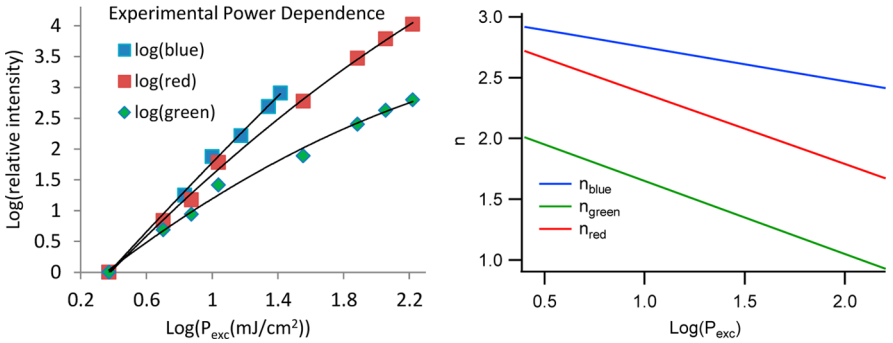

Figure 3. (Left) Logarithmic plot of the dependence of relative emission intensity of blue, green, and red upconversion on excitation power density (λ_{exc} = 943 nm) in β-$NaYF_4$:18%Yb, 2%Er powders. The trend lines through the data points are polynomial fits to the data. (Right) Exponential dependence, n, of emission intensity on log P_{exc} for blue, green and red upconversion. Values of n are the slopes of the polynomial fits, shown in the left panel, as a function of log P_{exc}.

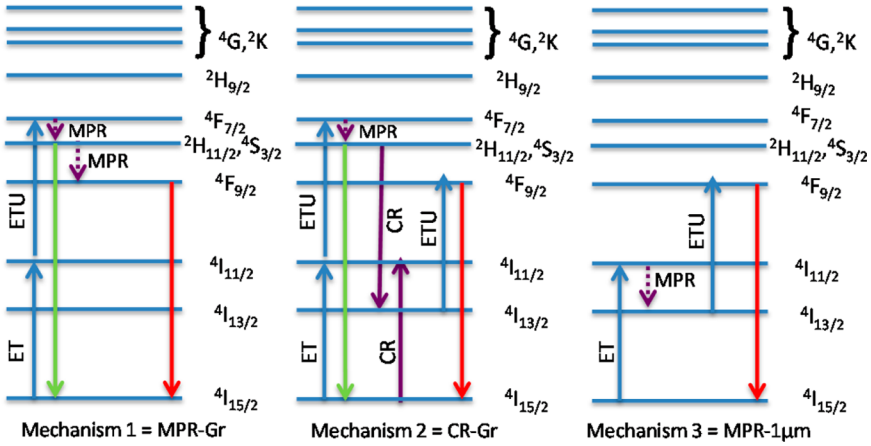

Figure 4. Three of the four proposed mechanisms for production of red UC luminescence. The first two mechanisms require energy transfer upconversion (ETU) for initial population of $^2H_{11/2}$,$^4S_{3/2}$, the green emitting states. The red emitting state, $^4F_{9/2}$ is then populated alternatively by multiphonon relaxation (MPR) or through ETU from $^4I_{13/2}$ following Er−Er cross-relaxation (CR). In the third mechanism, population of $^4I_{13/2}$ is achieved through MPR and subsequent ETU results in red emission.

to the green, as shown in Figure 5 (left panel). The right panel of Figure 5 shows the R/G ratio observed for the upconversion

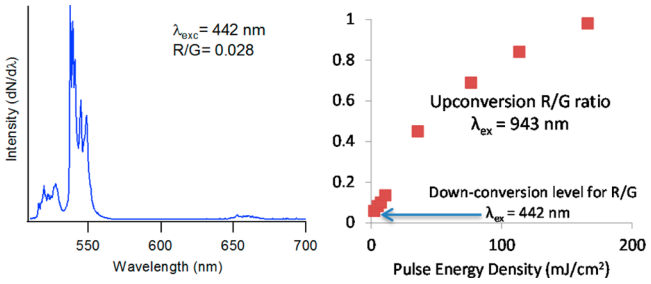

Figure 5. (Left) Downconversion emission spectrum of β-$NaYF_4$:18% Yb,2%Er powder excited at 442 nm. (Right) Red-to-green intensity ratio (R/G) as a function of excitation power density when using 943 nm excitation. The R/G value for the downconversion spectrum is indicated for comparison purposes.

process, exciting at 943 nm, as a function of excitation power density. The R/G ratio observed in the down conversion measurement (R/G = 0.028) is much lower than that observed in typical upconversion spectra. The R/G values for upconversion spectra approach that of downconversion only at very low values of P_{exc}. Furthermore, MPR would not show a dependence on excitation power, whereas the upconversion red-to-green ratio is highly dependent on the pump power density. Therefore, we conclude that MPR from the green emitting does not contribute significantly to red upconversion in $NaYF_4$:18%Yb^{3+},2%Er^{3+}, except when very low pump power densities are used and the observed R/G ratio is <0.2. This conclusion is in agreement with the recent work of Lee et al., regarding the highly efficient $NaYF_4$ UC host.[8] This is not to say that Mechanism 1 is not operable in oxide and oxyfluoride host materials where the higher phonon cutoff would be expected to lead to more efficient multiphonon relaxation.[13−15]

The second proposed mechanism (mechanism 2, Figure 4) also occurs through the initial population of the thermally coupled green emitting states, $^2H_{11/2}$ and $^4S_{3/2}$. Subsequent Er−Er cross-relaxation (CR) then populates $^4I_{13/2}$, which is converted to $^4F_{9/2}$ through Yb → Er energy transfer. This mechanism is consistent with the pump power density (P_{exc}) dependence of the red upconversion emission intensity (I), which suggests involvement of a three-photon process, approaching $I \propto (P_{exc})^{2.7}$ at low pump power densities.

Er−Er cross-relaxation occurs between adjacent Er^{3+} ions, in which one ion in the $^4S_{3/2}$ excited state transfers energy to a second ion in the ground state, $^4I_{15/2}$, resulting in both ions at intermediate levels of excitation, $^4I_{13/2}$ and $^4I_{11/2}$, as illustrated by the purple arrows in Figure 4, mechanism 2. This Er−Er cross-relaxation is a well-accepted process and is frequently

DOI: 10.1021/acs.jpca.5b08324
J. Phys. Chem. A 2015, 119, 9805−9811

cited in various contexts.[14−16] We also observe evidence for efficient Er−Er cross relaxation in $NaYF_4$:Yb^{3+},Er^{3+} at 1−3% Er doping levels. Figure 6 (top panel) illustrates the green

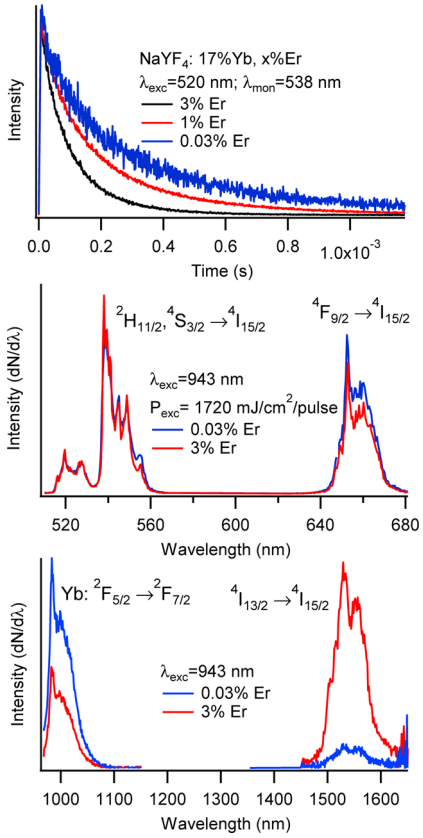

Figure 6. (Top) Decay curves of green emission (mon. 538 nm) following 520 nm excitation; (middle) visible and (bottom) NIR emission following 943 nm excitation for $NaYF_4$:*x*%Er,17%Yb nanoparticles in toluene.

luminescence decay curves for nanoparticles of $NaYF_4$:17% Yb^{3+},*x*%Er^{3+} (*x* = 3, 1, and 0.03) following excitation at 520 nm, directly into $^2H_{11/2}$. The decay constant for the green emitting state, *k*, increases significantly with increasing Er^{3+} concentration, from $k = 3000\ s^{-1}$ at 0.03%Er^{3+} to $k = 10\,000\ s^{-1}$ at 3% Er^{3+}. (We note that these decay constants, k, observed for the nanomaterials represented in Figure 6 are consistent with those observed for the micron-sized powders. See Supporting Information.) Moreover, a comparison of the NIR spectra for the 0.03%Er^{3+} and 3%Er^{3+} samples, when exciting at 943 nm, shows a dramatic relative increase in $^4I_{13/2} \rightarrow {}^4I_{15/2}$ emission at 1530 nm with increasing Er^{3+} concentration. This confirms that Er−Er cross relaxation occurs, and that it results in increased population of $^4I_{13/2}$, which is the proposed reservoir state for the final Yb → Er energy-transfer step in mechanism 2 that populates the red emitting state, $^4F_{9/2}$.

Thus, mechanism 2 is consistent with (1) the observed power dependence of red emission and (2) the established existence of an Er−Er cross-relaxation process that populates the $^4I_{13/2}$ reservoir state. However, mechanism 2 predicts that increasing Er−Er cross relaxation, that is, increasing the population of $^4I_{13/2}$, should lead to an increase in the red-to-green upconversion intensity ratio, R/G. As seen in the middle panel of Figure 6, in spite of the fact that Er−Er cross-relaxation is largely eliminated in the 0.03% Er^{3+} sample, the R/G ratio is similar to, or even slightly higher, than that in the 3% Er^{3+} sample. Therefore, the R/G upconversion intensity ratio is not diminished at low-Er doping concentration, proving that the Er−Er cross-relaxation step shown in mechanism 2 is not involved in the primary red upconversion mechanism. We conclude, then, that Er−Er cross relaxation does not play a significant role in the origin of red upconversion luminescence and that mechanism 2 (Figure 4), and any other mechanism invoking Er−Er can be discounted. Moreover, since it is established that the Er−Er CR process in mechanism 2 does effectively populate $Er^{3+}(^4I_{13/2})$ at concentrations typically used in UC materials, it is clear that it is the $Er^{3+}(^4I_{13/2}) \rightarrow Er^{3+}(^4F_{9/2})$ promotion via Yb-to-Er energy transfer (ETU) that does not occur to any significant extent. *Therefore, we conclude there are no efficient upconversion mechanisms in β-*$NaYF_4$:Yb,Er *that involve the* $Er^{3+}(^4I_{13/2})$ *state as a feeding state for red upconversion.*

In the third proposed mechanism, illustrated in Figure 4, multiphonon relaxation (MPR) from $^4I_{11/2}$ populates $^4I_{13/2}$, which results in excitation to $^4F_{9/2}$ and red emission, following Yb-to-Er ETU. As just discussed with regard to mechanism 2, however, we have shown that population of the $Er^{3+}(^4I_{13/2})$ state does not lead to red upconversion, so that mechanism 3 cannot be active.

The fourth mechanism, proposed by Anderson et al., is illustrated in Figure 7.[6] As with mechanisms 1 and 2, the

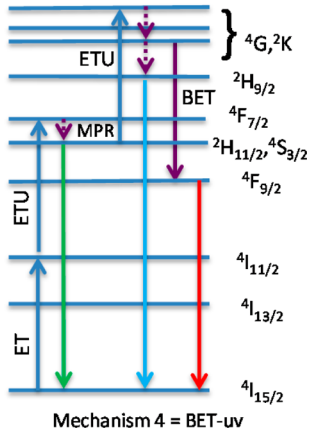

Figure 7. In the fourth proposed mechanism, the red emitting state is populated by back energy transfer (BET) from Er^{3+} in the $^4G,^2K$ manifold to ground state Yb^{3+}.

proposed red upconversion mechanism begins with the population of the green emitting states, $Er^{3+}(^2H_{11/2}, {}^4S_{3/2})$, via the accepted two-photon process discussed previously (See Figure 1). Subsequently, a third Yb → Er ETU step promotes the Er^{3+} from the long-lived green emitting states into a fairly dense manifold of states, labeled as $^4G/^2K$, that lie above the blue emitting state, $^2H_{9/2}$.

$$Er^{3+}(^2H_{11/2}, {}^4S_{3/2}) + Yb^{3+}(^2F_{5/2}) \rightarrow Er^{3+}(^4G/^2K) + Yb^{3+}(^2F_{7/2}) \quad (3)$$

After relaxing within the $^4G/^2K$ manifold, Er^{3+} can either undergo back energy transfer (BET) to Yb^{3+}, resulting in population of the $Er^{3+}(^4F_{9/2})$ red-emitting state, as expressed below

DOI: 10.1021/acs.jpca.5b08324
J. Phys. Chem. A 2015, 119, 9805−9811

$$Er^{3+}(^4G/^2K) + Yb^{3+}(^2F_{7/2}) \rightarrow Er^{3+}(^4F_{9/2}) + Yb^{3+}(^2F_{5/2}) \quad (4)$$

or, relax to the blue emitting state, $^2H_{9/2}$, via MPR.

$$Er^{3+}(^4G/^2K) \xrightarrow{MPR} Er^{3+}(^2H_{9/2}) \quad (5)$$

Interestingly, therefore, both red and blue upconversion proceed via the same three-photon excitation mechanism involving the green emitting state as an intermediate "reservoir". Whether red or blue emission is observed depends on the relaxation pathway out of $Er^{3+}(^4G/^2K)$: energy transfer or multiphonon relaxation. Anderson et al. showed that this mechanism is consistent with the observed power dependence of the intensity ratios and with the shapes of the luminescence decay curves for the red emission following pulsed NIR excitation. Here, we will argue for the validity of this mechanism using more direct spectroscopic evidence.

As stated above, according to mechanism 4, the red and blue upconversion mechanisms are closely related; it is most instructive first to consider that of the blue. The power dependence of the blue upconversion intensity is consistent with a three-photon process. (See Figure 3.) The upper panel in Figure 8 shows the time evolution of up- and down-

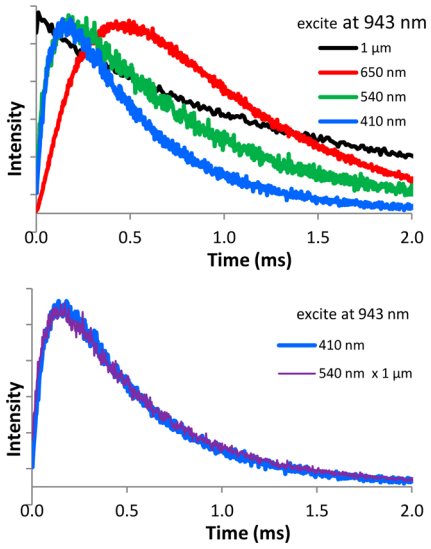

Figure 8. (Top) Time resolved luminescence for red, green, and blue UC emission, as well as 1 μm emission, following pulsed excitation at 943 nm. (Bottom) Superposition of the blue emission curve with the point-by-point product of the green and 1 μm emission curves.

conversion emission from $NaYF_4$:18%Yb,2%Er powder following pulsed 943 nm excitation. In the bottom panel of Figure 8, it is illustrated that the time dependence of the blue UC emission is nearly exactly reproduced by the product of the time dependence of the green and 1 μm luminescence. This strongly suggests that the $Yb^{3+}(^2F_{5/2})$ and $Er^{3+}(^2H_{11/2}, {}^4S_{3/2})$ excited states are the initial states in the energy transfer step leading to blue emission, consistent with steps 3 and 5 listed above. (Note: The shape of the blue time dependence also implies that step 5 and subsequent $Er^{3+}(^2H_{9/2})$ relaxation are fast relative to the time evolution of the green and NIR emission.)

We have, therefore, established that a three-photon mechanism, going through the green emitting state, populates the blue emitting state, $Er^{3+}(^2H_{9/2})$. Also, resonance considerations, as illustrated in Figure 7, suggest that Yb-to-Er ETU out of $^2H_{11/2}$, $^4S_{3/2}$ must populate $Er^{3+}(^4G/^2K)$ prior to population of $^2H_{9/2}$ through MPR. We will now establish that there is a branching pathway out of $Er^{3+}(^4G/^2K)$, competing with MPR to $^2H_{9/2}$, that directly populates the $Er^{3+}(^4F_{9/2})$ red emitting state (i.e., step 4).

Figure 9 compares the downconversion excitation spectra of $NaYF_4$:18%Yb,2%Er^{3+} powder monitoring green (552 nm) and

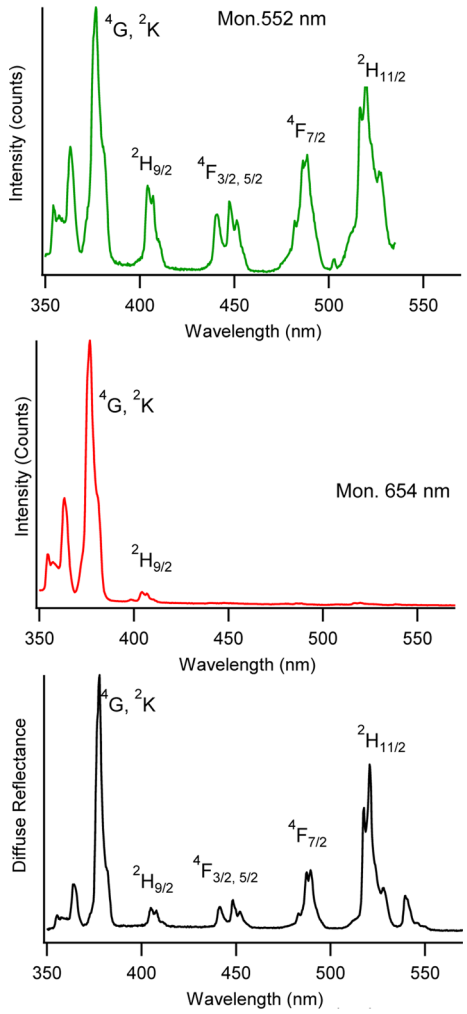

Figure 9. Downconversion excitation spectra of $NaYF_4$: 2%Er, 18%Yb powder monitoring green (top panel) and red (middle panel) emission at 552 and 654 nm, respectively. The bottom panel shows the Kubelka–Munk diffuse reflectance spectrum.

red (654 nm) emission. The diffuse reflectance spectrum is also given, so that all sample absorbance in this region can be seen. Excitation into all states at or above the $^2H_{11/2}$, $^4S_{3/2}$ manifold results in significant green emission. However, no significant red emission is produced until excitation into the $^4G/^2K$ manifold. These spectra show that there is no significant feeding of red emission directly from the green emitting state (as already discussed) and, more importantly, that there is an efficient pathway out of $^4G/^2K$ that feeds red emission. We will now demonstrate that this is a direct pathway, bypassing the blue emitting state, as well as the green.

The top panel of Figure 10 shows the downconversion emission spectrum of $NaYF_4$:18%Yb,2%Er^{3+} powder following

DOI: 10.1021/acs.jpca.5b08324
J. Phys. Chem. A 2015, 119, 9805−9811

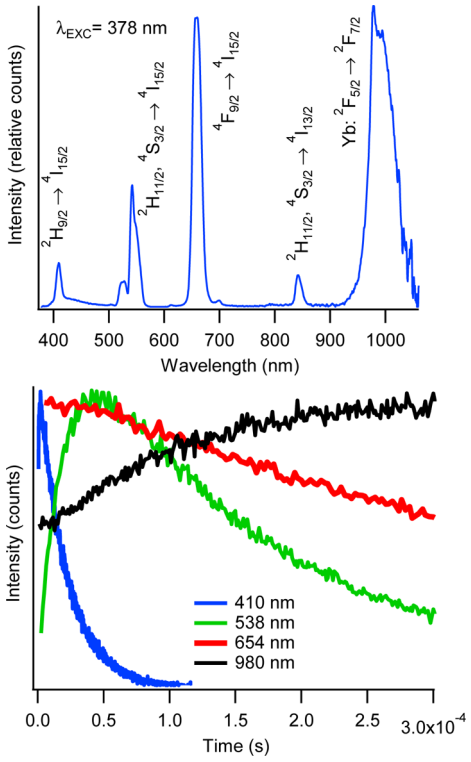

Figure 10. (Top) Down conversion emission spectrum and (bottom) emission decay curves of $NaYF_4$:2%Er,18%Yb powder exciting at 378 nm.

direct excitation into the $Er^{3+}(^4G/^2K)$ manifold at 378 nm. This excitation wavelength results in strong red emission, with a red-to-green ratio, R/G = 2.6, much higher than observed in any of the upconversion experiments (see Figure 5, right panel) or when exciting directly into the green emitting state (see Figure 5, left panel). This again reinforces our assertion that there is a branching path from $Er^{3+}(^4G/^2K)$ to the red emitting state, $^4F_{9/2}$, which bypasses the green emitting state, $^2H_{11/2}$, $^4S_{3/2}$, consistent with eq 4 in the proposed mechanism 4. Moreover, the red-to-blue intensity ratio (R/B ~ 20) measured for this down conversion experiment is similar to the red-to-blue ratio measured for moderate-power upconversion experiments, which is consistent with a common origin for population of the red and blue emitting states from the $^4G/^2K$ manifold, in both downconversion and upconversion measurements.

The luminescence decay curves following pulsed excitation at 378 nm (bottom panel of Figure 10) further support this interpretation. While a very fast rise is seen for blue, red, and NIR emission, green emission is characterized by a delayed luminescence, with a rise time consistent with the decay time of blue emission. The blue, red, and NIR emitting states are, therefore, all populated via fast relaxation pathways out of $Er^{3+}(^4G/^2K)$, corresponding to steps 4 and 5 above, and the green emitting state is populated subsequent to step 5 via relaxation from the blue emitting state. The immediacy of red and NIR emission prove that the relaxation to the corresponding emitting states from $Er(^4G/^2K)$ bypasses both the blue and green emitting states, and strongly supports the back energy transfer process, step 4, as the relevant pathway.

To summarize, the direct interpretation of a large body of spectroscopic data overwhelmingly supports the proposed mechanism of Anderson et al. for NIR-to-red and NIR-to-blue upconversion. Namely, both red and blue upconversion are produced primarily by a three-photon excitation process that proceeds through the green emitting state to a dense manifold of states ($^4G/^2K$) above the blue emitting state, $^2H_{9/2}$. Competing relaxation mechanisms out of $^4G/^2K$ determine the relative amounts of blue and red upconversion produced. Multiphonon relaxation from $^4G/^2K$ results in blue upconversion emission, whereas back energy transfer from $Er^{3+}(^4G/^2K)$ to $Yb^{3+}(^2F_{7/2})$ results in red emission.

CONCLUSION

Significant discrepancies exist in the literature regarding the mechanism whereby red emission is generated in the NIR-to-visible upconversion process in $NaYF_4$ codoped with Yb^{3+} and Er^{3+}. For the most part, the proposed mechanisms have not been critically tested, but, instead, have been offered as reasonable hypotheses based on limited data sets. Here we demonstrate that the most commonly invoked mechanisms are not significant contributors to the red emission, whereas a more recently proposed mechanism is consistent with all available data. Specifically, we have demonstrated that the strong red emission does not arise from MPR from $^4S_{3/2}$ down to $^4F_{9/2}$. Nor does the red emission arise from promotion of Er^{3+} from $^4I_{13/2}$ to $^4F_{9/2}$ through Yb → Er ETU. A different mechanism, involving a three-step ETU process, exciting Er^{3+} to the $^4G/^2K$ manifold, followed by a single Er → Yb back energy transfer step to populate $Er^{3+}(^4F_{9/2})$, is consistent with all of the data and deserves further consideration as the only current viable mechanism in this material.

ASSOCIATED CONTENT

Supporting Information

The Supporting Information is available free of charge on the ACS Publications website at DOI: 10.1021/acs.jpca.5b08324.

Luminescecence decay analysis with a figures showing the average decay rate (PDF)

AUTHOR INFORMATION

Corresponding Author

*(M.T.B.) E-mail: Mary.Berry@usd.edu.

Notes

The authors declare no competing financial interest.

ACKNOWLEDGMENTS

The authors acknowledge support from NSF (EPS-0903804) and the State of South Dakota, Governor's Office of Economic Development. P.S.M. acknowledges support from NASA (Cooperative Agreement Number:NNX10AN34A).

REFERENCES

(1) Heer, S.; Kömpe, K.; Güdel, H.-U.; Haase, M. Highly Efficient Multicolour Upconversion Emission in Transparent Colloids of Lanthanide-Doped $NaYF_4$ Nanocrystals. *Adv. Mater.* **2004**, *16*, 2102−2105.

(2) Pokhrel, M.; Gangadharan, A. K.; Sardar, D. K. High Upconversion Quantum Yield at Low Pump Threshold in Er^{3+}/Yb^{3+} Doped La_2O_2S Phosphor. *Mater. Lett.* **2013**, *99*, 86−89.

(3) Auzel, F. Compteur Quantique par Transfert d'Energie Entre de Yb^{3+} a Tm^{3+} dans un Tungstate Mixte et dans Verre Germinate. *C. R. Acad. Sci. (Paris)* **1966**, *263*, 819−821.

(4) Auzel, F. Upconversion and Anti-Stokes Processes with f and d Ions in Solids. *Chem. Rev.* **2004**, *104*, 139−174.

DOI: 10.1021/acs.jpca.5b08324
J. Phys. Chem. A 2015, 119, 9805−9811

(5) Suyver, J. F.; Grimm, J.; Krämer, K. W.; Güdel, H. U. Highly Efficient Near-Infrared to Visible Up-Conversion Process in $NaYF_4:Er^{3+},Yb^{3+}$. *J. Lumin.* **2005**, *114*, 53−59.
(6) Anderson, R. B.; Smith, S. J.; May, P. S.; Berry, M. T. Revisiting the NIR-to-Visible Upconversion Mechanism in β-$NaYF_4:Yb^{3+}$, Er^{3+}. *J. Phys. Chem. Lett.* **2014**, *5*, 36−42.
(7) Suyver, J. F.; Grimm, J.; van Veen, M. K.; Biner, D.; Krämer, K. W.; Güdel, H. U. Upconversion Spectroscopy and Properties of $NaYF_4$ doped with Er^{3+}, Tm^{3+} and/or Yb^{3+}. *J. Lumin.* **2006**, *117*, 1−12.
(8) Jung, T.; Jo, H. L.; Nam, S. H.; Yoo, B.; Cho, Y.; Kim, J.; Kim, H. M.; Hyeon, T.; Suh, Y. D.; Lee, H.; Lee, K. T. The Preferred Upconversion Pathway for the Red Emission of Lanthanide-doped Upconverting Nanoparticles, $NaYF_4:Yb^{3+},Er^{3+}$. *Phys. Chem. Chem. Phys.* **2015**, *17*, 13201−13205.
(9) Dong, H.; Sun, L.-D.; Wang, Y.-F.; Ke, J.; Si, R.; Xiao, J.-W.; Lyu, G.-M.; Shi, S.; Yan, C.-H. Efficient Tailoring of Upconversion Selectivity by Engineering Local Structure of Lanthanides in Na_xREF_{3+x} Nanocrystals. *J. Am. Chem. Soc.* **2015**, *137*, 6569−6576.
(10) Xiang, G.; Zhang, J.; Hao, Z.; Zhang, X.; Pan, G.-H.; Luo, Y.; Lü, W.; Zhao, H. Importance of Suppression of Yb^{3+} De-Excitation to Upconversion Enhancement in β-$NaYF_4$: $Yb^{3+}/Er^{3+}@\beta$-$NaYF_4$ Sandwiched Structure Nanocrystals. *Inorg. Chem.* **2015**, *54*, 3921−3928.
(11) Paudel, H. P.; Zhong, L. L.; Bayat, K.; Baroughi, M. F.; Smith, S.; Lin, C. K.; Jiang, C. Y.; Berry, M. T.; May, P. S. Enhancement of Near-Infrared-to-Visible Upconversion Luminescence Using Engineered Plasmonic Gold Surfaces. *J. Phys. Chem. C* **2011**, *115*, 19028−19036.
(12) Suyver, J. F.; Aebischer, A.; García-Revilla, S.; Gerner, P.; Güdel. Anomalous Power Dependence of Sensitized Upconversion Luminescence. *Phys. Rev. B: Condens. Matter Mater. Phys.* **2005**, *71*, 125123.
(13) Feng, L.; Wang, J.; Tang, Q.; Hu, H.; Liang, H.; Su, Q. Optical Proerties of Er^{3+} - singly doped and Er^{3+}/Yb^{3+} -codoped novel oxyfluoride glasses. *J. Non-Cryst. Solids* **2006**, *352*, 2090−2095.
(14) Patra, A.; Friend, C. S.; Kapoor, R.; Prasad, P. N. Fluorescence Upconversion Properties of Er^{3+}-Doped TiO_2 and $BaTiO_3$ Nanocrystallites. *Chem. Mater.* **2003**, *15*, 3650−3655.
(15) Patra, A.; Friend, C. S.; Kapoor, R.; Prasad, P. N. Upconversion in $Er^{3+}:ZrO_2$ Nanocrystals. *J. Phys. Chem. B* **2002**, *106*, 1909−1912.
(16) Quimby, R. S.; Miniscalco, W. J.; Thompson, B. Clustering in Erbium-doped Silica Glass Fibers Analyzed Using 980 nm Excited-state Absorption. *J. Appl. Phys.* **1994**, *76*, 4472.

DOI: 10.1021/acs.jpca.5b08324
J. Phys. Chem. A 2015, 119, 9805−9811